

GNN-based Passenger Request Prediction

Aqsa Ashraf Makhdomi and Iqra Altaf Gillani

Department of Information Technology, NIT Srinagar

ARTICLE HISTORY

Compiled January 26, 2024

ABSTRACT

Passenger request prediction is essential for operations planning, control, and management in ride-hailing platforms. While the demand prediction problem has been studied extensively, the Origin-Destination (OD) flow prediction of passengers has received less attention from the research community. This paper develops a Graph Neural Network (GNN) framework along with the Attention Mechanism to predict the OD flow of passengers. The proposed framework exploits various linear and non-linear dependencies that arise among requests originating from different locations and captures the repetition pattern and the contextual data of that place. Moreover, the optimal size of the grid cell that covers the road network and preserves the complexity and accuracy of the model is determined. Extensive simulations are conducted to examine the characteristics of our proposed approach and its various components. The results show the superior performance of our proposed model compared to the existing baselines.

KEYWORDS

Ride-hailing; Route recommendation; Demand prediction; OD prediction; GNN; Context-aware data

1. Introduction

The rapid growth of GPS-enabled services and location-based sensors has resulted in an enormous volume of geo-tagged data which provides information about passenger mobility patterns and vehicular movement. This data about passenger arrival and departure from different locations can be analyzed and the patterns can be exploited among them in order to predict the future areas that will fetch more requests. This will help the ride-hailing platforms in assigning the requests of nearby passengers to the drivers. It will ultimately decrease the waiting time of passengers and the cruising distance of drivers without having a passenger in the vehicle. The decrease in cruising distance of vehicles results in more profit for the platform as the passengers are fetched earlier on the route. It further has a positive impact on the environment as there is a reduction in the emission of greenhouse gases, owing to the decrease in distance travelled by the vehicle. Thus the prediction of requests enhances the service quality of ride-hailing platforms and contributes to a greener environment. This is an important area of research and the output of these prediction techniques is used as input by various route recommendation Garg & Ranu (2018) and matching algorithms Gao, Li, Wang, & Huang (2022). It has gathered significant attention from researchers and a

number of works like Jin et al. (2020); Wang et al. (2021a) have been done that have predicted the areas with more passenger demand.

Most of the works Jin et al. (2020); Wang et al. (2021a) that have been done in this direction have predicted the areas that will fetch more requests, which is also called demand prediction. However, the mobility patterns of passengers can be better analyzed if the origin (the place from where the request came), as well as the destination (the place to which the request is headed) of requests, can be predicted simultaneously and not only their origin. This is particularly useful for ridesharing platforms (platforms that enable multiple passengers to share a single ride) where the efficient pairing of passengers can be done if the origin and destination of passengers are known beforehand. It is a new area of interest and various models have been proposed to predict the Origin-Destination (OD) pair. Some of the studies have explored the application of statistical models Cho, Myers, & Leskovec (2011) for prediction, but their accuracy is below 50% which can be attributed to the complex spatio-temporal dependencies inherent in request data. These dependencies have been effectively captured by employing a range of deep-learning models Schaller (2021); Seo, Defferrard, Vandergheynst, & Bresson (2018); Shen, Tziritas, & Theodoropoulos (2022); Wang et al. (2019, 2021b). Among them, Graph Neural Networks (GNNs) Seo et al. (2018); Shen et al. (2022); Wang et al. (2019, 2021b) have gained prominence over Convolutional Neural Networks (CNNs) due to their capability to account for non-euclidean distances among neighboring data points. All of these models capture the linear trends in data that occur due to the repeating schedules of passengers. However, apart from linear trends, there can be non-linear trends in data.

Our proposed model, in addition to these linear patterns, also aims to capture non-linear patterns that may result in dependencies between requests. It uses GNN to model the underlying road network with different linear and non-linear dependencies among the ride-hailing requests. The linear trends in data are determined through the data from the same or consecutive hours of the preceding time frames. Whereas the non-linear patterns in data are determined by taking the aggregate information from the data of the preceding hours. This data provides insights into the behavioral patterns of people and describes the contextual information of that place. For instance, if the requests from the preceding hours are low in quantity, it reveals that either the area is sparse in requests or some event has occurred that has reduced the flow of requests to that area. Moreover, these dependencies also reflect the travelling behavior of people and thereby indicate the re-appearance of requests after a period of time. For instance, requests start to recur after office hours of people are finished or they have completed the time spent outside their homes. These dependencies are captured by analyzing the data from previous hours and determining the time frame after which requests tend to re-appear.

Grid size is a crucial factor to consider when modelling these dependencies since it determines the number of spatial and temporal neighbors at a given time. When the grid size is large, the neighborhood count decreases which results in the inability to account for spatio-temporal dependencies. On the other hand, small grid sizes make it necessary to retain microscopic features, which ultimately leads to an increase in the complexity of the model. Thus, the appropriate grid size which captures the passenger mobility accurately in a time-bound manner is a parameter that needs to be determined.

Our major contributions can be summarized as follows:

- We model the ride-hailing network as a graph and use GNN to capture the com-

- plex spatio-temporal dependencies among the requests that arrive from different locations and varying time frames.
- We determine the temporal functioning of ride-hailing platforms and explore non-linear patterns that appear within the request sequences.
 - The proposed model displays that apart from the periodic trends in data, the dependencies among requests can arise due to the movement and behavioral patterns of people.
 - We determine the optimal size of the grid cell considering the complexity and accuracy of the model.
 - We conduct extensive simulations using a real-world dataset to empirically validate the effectiveness of our proposed model. The superior performance demonstrated in these simulations showcases the practical utility and relevance of our approach in ride-hailing platforms.

The rest of the paper is organized as follows: In Section 2, a review of the existing work done related to the request prediction is presented. In Section 3, the preliminaries required to understand our proposed model are described. In Section 4 the details of the proposed model are discussed. In Section 5, the dataset, evaluation metrics, results, and comparison of algorithms is discussed. Section 6 highlights the key applications of the proposed model in ride-hailing industry. Finally, Section 7 concludes our work and highlights its key contributions.

2. Related Work

Ride-hailing services like Ola and Uber generate an enormous volume of data, which includes information about trajectories, geo-tagged check-ins, and ride sources and destinations. The patterns among data can be learned and understood for the advanced development of these services in recommending optimal routes Garg & Ranu (2018) or providing matching algorithms Gao et al. (2022) to drivers and passengers. Various machine learning and deep learning-based models have been used to understand the patterns among data and utilize those patterns for future prediction of requests Han, Song, Wang, et al. (2004); Wang et al. (2021b). These prediction algorithms for ride-hailing platforms work in two-fold directions: predicting the demand at nodes and predicting the OD pair of requests. Demand prediction methods predict the number of requests that will arrive at a node and the OD-based prediction methods predict the number of requests that will arrive between a specified origin and destination pair of vertices.

Various works have been in the direction of demand prediction. These works have evolved from pure time series-based models Han et al. (2004); Lippi, Bertini, & Frasconi (2013) to the models exploiting spatial and temporal dependencies Jin et al. (2020); Wang et al. (2021a). The time series-based models exploit the temporal patterns in data and based on these predict the future areas that will have more requests. Since ride-hailing requests depend upon both the spatial and temporal dependencies, some of the recent research works have started to exploit both these dependencies by using various machine learning and deep learning-based approaches Han et al. (2004); Wang et al. (2021b).

Recently, OD prediction has arisen as a potential topic among researchers as it can enhance the functionality of ride-hailing platforms, in particular ridesharing systems. Various works have been done that have used GNN based models to predict

the origin and destination of requests Hamilton, Ying, & Leskovec (2017); Shen et al. (2022); Wang et al. (2019, 2021b). In this direction, Hamilton *et al.* Hamilton et al. (2017) proposed a general induction framework, GraphSAGE, that used the attribute information to create node embeddings for the vertices of the graph. However, their proposed model only focused on spatial dependencies and did not capture the temporal patterns in the data. Wang *et al.* Wang et al. (2019) proposed a grid embedding-based multi-task learning framework, where the grid embedding models the spatial dependencies that can arise among requests from different areas, and LSTM-based multi-task learning framework captures the temporal dependencies in the data. However, their proposed model did not consider the direction of the flow of requests and they considered the requests that originate at node v or are destined to node v as the same. This could affect the performance of the system considerably. For instance, if the requests are moving from their homes to shopping malls the direction of movement of requests is an important pattern and its ignorance can affect the system’s performance significantly. In order to overcome the above problems, Wang *et al.* Wang et al. (2021b) proposed a representation learning-based OD prediction model that leveraged the spatial and temporal dependencies through the use of three types of neighbors: forward, backward, and geographical. Their proposed model took the directed nature of requests into account and accordingly considered the neighbors as forward or backward based upon their precedence of request. Apart from these models, other works Hu et al. (2023); Ke et al. (2021); Shen et al. (2022) have been done that have used multi-graph attention and federated learning-based models to find the dependencies among requests and accordingly predicted the origin and destination of future requests.

All of the above works model the dependencies that arise due to the repeating trends in data. However, apart from these recurring trends, there can be dependencies due to the non-recurring patterns in data. Our proposed model tries to overcome the above limitations and capture the spatial and temporal dependencies, in particular the dependencies that appear due to non-repeating patterns like contextual data or the travelling behavior of people. It is based on the architecture proposed by Wang et al. (2021b) and Shen et al. (2022).

3. Preliminaries

In this section, we will discuss the preliminaries associated with our proposed model.

Grid

Our proposed model assumes that the entire city is divided into n non-overlapping grid cells, denoted by $g = \{g_1, g_2, \dots, g_n\}$. The grid cell represents a geographic area and is defined by its latitude and longitude coordinates. The distance between adjacent grid cells is measured between their central (middle) points. For each cell of the grid, we predict the number of requests that originate from there and are headed toward other cells. Figure 1 shows the example of a road network divided in terms of grid cells. The grid has 25 cells and each cell i of the grid is defined by its grid ID g_i where $i \in [1, 25]$. Our proposed model predicts the number of requests that can arrive between any two cells of the grid. Their value is stored in the OD matrix, where the rows and columns of the matrix denote the grid cells and the entry of the matrix represents the number of requests that can arrive between those cells. Figure 2 shows the OD matrix corresponding to the grid described in Figure 1. As can be seen through Figure 2, each entry of the matrix contains the number of requests (Δ_{ij}) that can arrive between the i^{th} cell of the grid (g_i) and the j^{th} cell of the grid (g_j), where $i, j \in [1, 25]$.



Figure 1.: Road network represented in the form of a grid

Time Slots

We split time into 24 distinct slots $t = \{t_1, t_2, \dots, t_{24}\}$ where t_i represents the time between the i^{th} and $(i - 1)^{\text{th}}$ hour. For instance, t_1 corresponds to the time between 12 : 00 A.M. and 1 : 00 A.M..

Spatio-temporal dependencies

The requests in ride-hailing platforms have temporal dependencies as the studies have found that there are regular time-based patterns among requests that could be exploited for further prediction. For instance, during morning hours, the requests follow the pattern of having a destination at the office, and during the evening hours, requests originate from the office. These patterns can be used to predict the future origin and destination of requests.

Requests also follow spatial dependencies and depend upon the inflow and outflow of requests from the following areas, i.e., if the neighborhood region has high requests, it is highly probable that the current region will have more requests. Similarly, if a region is sparse in requests, its subsequent regions will certainly have few requests.

4. System model

In this section, we detail the working of our proposed architecture. As can be seen through Figure 3, input to our proposed model is a dataset that contains the request sequence $R = \{r_1, r_2, \dots, r_m\}$ of ride-hailing platforms, where r_i represents a particular request and m denotes the total number of requests. Each request is represented as $r_i = \langle r_{s_i}, r_{d_i}, r_i^{t'} \rangle$, where r_{s_i} and r_{d_i} determine the source and destination of request i respectively, and $r_i^{t'}$ represents the time at which the request i is made. This data is pre-processed and divided into 24 slots of 1-hour for each day and a graph $G = (V, E, \Delta)$ is created for each time slot. The vertices V of the graph denote the grid cells and the edges E represent the interconnections between different grid cells. This graph is a complete graph as requests can arrive between any pair of vertices. The adjacency matrix of the graph G is represented by the OD matrix shown in Figure 2. Each edge of the graph G is associated with a weight Δ_{ij} that determines the number of requests

Grid cell	g_1	g_2	.	g_j	g_{25}
g_1	1	2	.	3	1
g_2	0	2	.	2	0
.
g_i	1	2	.	Δ_{ij}	1
g_{25}	0	1	.	3	2

Figure 2.: OD Matrix of the grid

between the grid cells g_i and g_j . If there are no requests between the two vertices, the corresponding weight is set as 0. The output of the pre-processed stage is a sequence of graphs $G = \{G_1, G_2, \dots, G_{24}\}$, where G_i represents the requests that arrive in the t_i^{th} time slot i.e, all the requests that arrive between $(i-1)^{\text{th}}$ and i^{th} hour of the day. This graph sequence is generated for all the days in the dataset.

Each vertex of the graph is represented by an *embedding* which is its transformation into a vector space that describes it completely and preserves the maximal information about the local structure of the graph (connection between nodes and edges). In our proposed model the initial embedding of a vertex is a combination of its grid ID (g_i for the cell i of grid), row number, column number, time slot t_i , day of the week, in-degree, and out-degree. The in-degree and out-degree of a node are calculated from the OD matrix. If we represent each element of the OD matrix as $OD(g_i, g_j)$ where g_i represents the row grid cell and g_j represents the column grid cell as can be seen through Figure 2, then the in-degree of the grid cell g_k is $\sum_{i=1}^n OD(g_i, g_k)$ and its out-degree is $\sum_{j=1}^n OD(g_k, g_j)$. Initially, the embeddings of a node contain the local information associated with the node and edge connections. This information is unstable as it only provides a view of the local neighborhood and does not provide any indication of the spatial or temporal dependencies that can arise among the requests. In order to capture the dependencies among the requests and obtain a global view of the network, the nodes exchange embeddings with their spatial and temporal neighbors. These neighbors are selected by the following two layers of our proposed model: *spatial attention layer* - which selects the spatial neighbors and the *temporal attention layer* - which selects the temporal neighbors. After the final embeddings are calculated through these two layers, we need to predict the demand ($\hat{\delta}_i$) that can arrive at the i^{th} grid cell and the number of requests ($\hat{\Delta}_{ij}$) that may arrive between the i^{th} and j^{th} grid cells. Here $\hat{\delta}_i$ and $\hat{\Delta}_{ij}$ correspond to the predicted demand at grid cell i and the predicted number of requests between grid cells g_i and g_j respectively. Whereas δ_i and Δ_{ij} represent the actual demand at grid cell i and the actual number of re-

Notation	Description
g	Grid
g_i	i^{th} grid cell
t	Time Slots
t_i	i^{th} time slot
R	Request sequence
r_i	i^{th} request
r_{s_i}, r_{d_i}	Source and destination of request i
r_i^t	Time at which request i arrives
G	Request Graph
OD Matrix	Adjacency matrix of G
V	Vertices of graph G
E	Edges of graph G
G_i	Graph G at t_i time slot
$\Delta_{ij}, \hat{\Delta}_{ij}$	Actual and predicted number of requests between grid cells g_i and g_j
$\delta_i, \hat{\delta}_i$	Actual and predicted number of requests at grid cell g_i
f_j^t, b_i^t, q_i	Set of forward, backward, and geographical neighbors of grid cell g_i at time t
e_i^t	Embedding of node v_i at time t
W_c, W_s	Learnable weight matrices
w'	Pre-weighted aggregator
Y	Vector that concatenates the embedding of neighboring nodes
a	Attention coefficient which maps a vector to a single number
μ	<i>LeakyReLU</i> activation function
$f_{ij}^t, b_{ij}^t, q_{ij}^t$	Weight of forward, backward and geographical neighbors when embeddings are exchanged
$\alpha_j^t, \beta_j^t, \gamma_j^t$	Pre-weighted aggregator for forward, backward and geographical neighbors
D	Graph that stores distance between different grid cells
d_{ij}	Distance between grid cells g_i and g_j
h	Number of hours for which non-linearity is determined
W^K, W^Q, W^V	Learnable weight matrices called as key, value and query matrices respectively
E^t, E_i^{t+1}	Spatial and initial embeddings of n grid cells at time slot t and $t + 1$ respectively
S	Similarity matrix
S', S''	Scaled and normalized similarity matrices
p_{ij}	Probability that requests are transferred from grid cell g_i to grid cell g_j
m	Total number of requests
n	Total number of grids

Table 1.: Notations

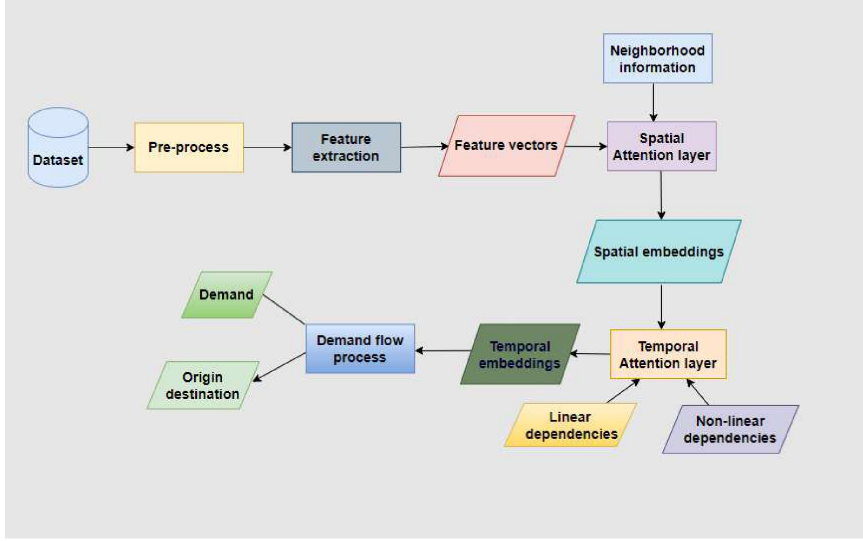


Figure 3.: Framework of our proposed model

quests between grid cells g_i and g_j respectively. We get the demand at a node and the number of requests between two nodes by feeding the result of these two layers to the *transferring attention layer*. The working of these layers is described in detail in the next subsections.

4.1. Spatial Attention Layer

After the initial embedding of nodes is created, it is fed as input to the spatial attention layer which produces a new embedding that carries information about all the spatial neighbors. These embeddings are created by exchanging data with three different types of spatial neighbors:

Forward neighbors - If there are two neighbors g_i and g_j , and there is at least one request that originates from g_i and is destined to g_j ($\Delta_{ij} > 0$) then g_j is the forward neighbor of g_i . The set of forward neighbors of g_i at time slot t is defined mathematically as:

$$f_i^t = \{g_j | \Delta_{ij}^t > 0, \Delta_{ij}^t \in G_t\} \quad (1)$$

Backward neighbors - If there are two neighbors g_i and g_j , and there is at least one request that originates from g_j and is destined to g_i then g_j is the backward neighbor of g_i . The set of backward neighbors of g_i at time slot t is defined mathematically as:

$$b_i^t = \{g_j | \Delta_{ji}^t > 0, \Delta_{ji}^t \in G_t\} \quad (2)$$

The sequential flow of requests in the network is captured by the forward and backward

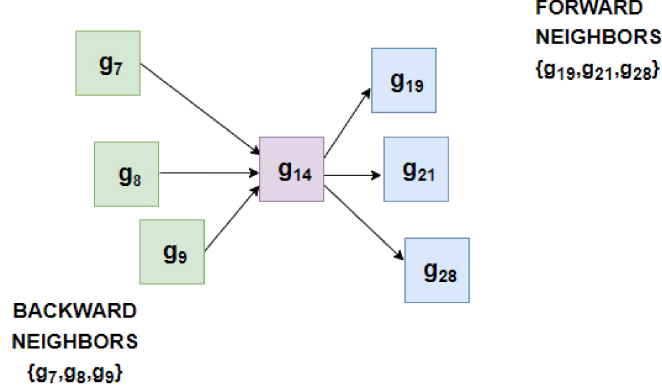


Figure 4.: Forward and backward neighbors calculated from an instance of graph G

neighbors, which are also referred to as semantic neighbors. These neighbors identify passenger mobility patterns and determine the flow of requests into and out of the specific region. These neighbors are time-dependent, as the request flow in a region is not constant across different time slots. They are calculated from an instance of graph G .

Figure 4 shows the set of forward and backward neighbors of the grid cell g_{14} at a particular time slot. The forward neighbors determine the out-flow of requests from a particular grid cell and the backward neighbors determine the in-flow of requests to a particular grid cell. As can be seen through Figure 4, $\{g_{19}, g_{21}, g_{28}\}$ is the set of forward neighbors of grid cell g_{14} as there are some requests that originate from g_{14} and are destined towards g_{19} , g_{21} and g_{28} respectively. Similarly $\{g_7, g_8, g_9\}$ is the set of backward neighbors of grid cell g_{14} as the requests from grid cells g_7, g_8 and g_9 have their destination at grid cell g_{14} .

Geographical neighbors - Two neighbors g_i and g_j are said to be geographically connected if the Haversine distance between their corresponding latitude/longitude pairs is within a specified threshold distance.

$$q_i = \{g_j | d_{ij} \leq L, d_{ij} \in D\} \quad (3)$$

where L is the threshold distance that determines the size of geographical neighbors and D is the distance graph that represents the distance (d_{ij}) between the central points of grid cells g_i and g_j . For instance, if we consider the part of the road network represented in the form of a grid by Figure 2, where the threshold distance is set to be equal to the length of one grid cell, then the set of geographical neighbors of grid cell g_{14} are is $\{g_8, g_9, g_{10}, g_{13}, g_{15}, g_{18}, g_{19}, g_{20}\}$. The set of geographical neighbors of g_i is constant across all time slots.

The geographical neighbors can be used to aggregate uncertainty in information

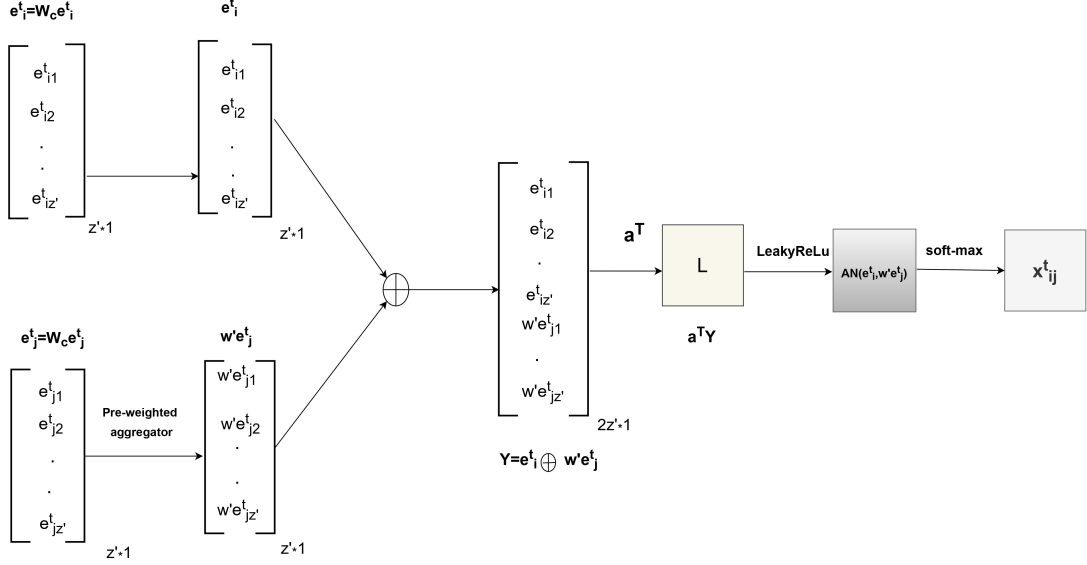


Figure 5.: Graph Attention Network for calculating affinity between neighboring nodes

from the areas with few requests (sparse areas). As we know requests arrive in negligible quantity in sparse areas, and the forward and backward neighbors capture the dependencies between the neighbors based on the request flow of a particular region. But, if a region is sparse in requests it will not have in-flow and out-flow of requests. In that case, there is no information from forward and backward neighbors. However, geographical neighbors are always there and can be used to exchange embeddings in that area.

The initial embeddings of nodes are fed as input to the Graph Attention Network (GAT) which combines the information from the three neighbors described above and represents it in the form of a unified vector e_i^t for each node v_i at time t . Some of the earlier models have used Graph Convolution Network (GCN) Hamilton et al. (2017) for combining information from different neighbors. However, with GCN all neighbors are assigned the same weightage when embeddings are merged, which neglects the importance of nodes that have a similar flow of requests or that are close to each other. We propose to use GAT which samples different neighbors based on their weight. It assigns a higher value to the geographical nodes that are in the close vicinity of the current node. Similarly, it provides more weightage to the semantic neighbors with a higher flow of requests to/from the current node. In this way, embeddings of nodes that have more information are prioritized and the noise from redundant nodes is removed.

In order to calculate the importance of a neighborhood node v_j at time t , we pass the embedding of the current node $e_i^t \in \mathcal{R}^{z \times 1}$ and the neighborhood node $e_j^t \in \mathcal{R}^{z \times 1}$ through a weight matrix $W_c \in \mathcal{R}^{z' \times z}$, where $z' > z$. This weight matrix acts as a single-layer neural network and projects the embedding of a node to a higher dimension. The output of this layer is the updated embedding of the nodes v_i and v_j at time t and they are equal to

$$e_i^t = W_c e_i^t \quad (4)$$

$$e_j^t = W_c e_j^t \quad (5)$$

where $e_i^t \in \mathcal{R}^{z' \times 1}$ and $e_j^t \in \mathcal{R}^{z' \times 1}$. Figure 5 displays the working of the attention-based aggregator of GAT. The input to GAT is the embedding e_i^t and e_j^t of nodes v_i and v_j at time t , after they have been passed through weight matrix W_c . The embedding e_j^t is passed through a pre-weighted aggregator w' which provides a prior weight to it before the GAT calculates its importance. This prior weight is based upon the current state of neighbors and is described in detail in the next subsection. The embedding e_i^t of node i and the embedding of the neighborhood node after being passed through a pre-weighted aggregator ($w' e_j^t$) are concatenated and represented as a single vector Y :

$$Y = e_i^t \oplus w' e_j^t \quad (6)$$

This vector is then passed through a learnable attention coefficient $a \in \mathcal{R}^{2z' \times 1}$ which maps it to a single number. Thereafter, non-linearity is applied through the *LeakyReLU* activation function denoted as μ in Eq.(7).

$$AN(e_i^t, w' e_j^t) = \mu(a^T Y) \quad (7)$$

This attention-based aggregator function of GAT measures the affinity between the embedding of node v_i and its neighbor v_j at time t by learning the weight matrix W_c and the attention coefficient a , and produces a single number that determines the weight of neighborhood node v_j when it needs to exchange embedding with the node v_i .

However, the output of the neural network is not normalized, which is a problem since the weights should be on the same scale for exchanging embeddings. In order to normalize the weights, we apply the soft-max function to the output of the attention-based aggregator defined in Eq. (7) which brings all the weights to the same scale. In Figure 5, these normalized weights are denoted as x_{ij}^t and they represent the weights of forward neighbors (f_{ij}^t), backward neighbors (b_{ij}^t), and geographical neighbors (g_{ij}). They are mathematically represented as

$$\begin{aligned} f_{ij}^t &= \frac{\exp(AN(e_i^t, \alpha_j^t e_j^t))}{\sum_{k \in f_i^t} \exp(AN(e_i^t, \alpha_k^t e_k^t))} \\ b_{ij}^t &= \frac{\exp(AN(e_i^t, \beta_j^t e_j^t))}{\sum_{k \in b_i^t} \exp(AN(e_i^t, \beta_k^t e_k^t))} \\ q_{ij}^t &= \frac{\exp(AN(e_i^t, \gamma_j e_j^t))}{\sum_{k \in q_i^t} \exp(AN(e_i^t, \gamma_k e_k^t))} \end{aligned} \quad (8)$$

These weights allow our proposed model to prioritize embeddings that are geographically and semantically similar to the node v_i at time t . Here, α_j^t , β_j^t , and γ_j refer to the pre-weighted functions which are detailed in the next subsection.

Since we have obtained the weights that determine the importance of each node, we exchange embeddings with the set of forward, backward, and geographical neighbors

with the weights f_{ij}^t , b_{ij}^t and q_{ij}^t calculated above as:

$$e_i^t = W_s e_i^t \oplus \sum_{j \in f_i^t} f_{ij}^t W_s e_j^t \oplus \sum_{j \in b_i^t} b_{ij}^t W_s e_j^t \oplus \sum_{j \in q_i} q_{ij}^t W_s e_j^t \quad (9)$$

Here e_i^t is the final embedding of each node v_i at time t and it is obtained by merging information from different sets of neighbors based upon their weights and W_s is the shared weight matrix that projects all embeddings onto the same z' dimensional space before merging them. Thereafter, they are passed through multi-head attention and head gates Shen et al. (2022) in order to capture the relationship between grids.

4.1.1. Pre-weighted aggregator

The pre-weighted aggregator provide a prior weight to the embedding of node v_j at time t before its affinity is measured by the attention-based aggregator defined in Eq. (7). The aggregator determines the current flow of requests, which is calculated from the edges (Δ_{ij}) of the graph G_t , and the geographical relationship between requests, which is determined through the edges (d_{ij}) of graph D . It allows our proposed model to sense the sparsity or density of requests in the current time slot and accordingly aggregate the information from the forward and backward neighbors that have a higher flow of requests. It also provides an indication of the geographical neighbors which are closer to the requests that arrive at time t . These pre-weighted aggregators are represented as α_j^t , β_j^t and γ_j for the forward, backward and geographical neighbors respectively and are defined as:

$$\begin{aligned} \alpha_j^t &= \frac{\Delta_{ij}}{\sum_{j \in f_i^t} \Delta_{ij} + s} \\ \beta_j^t &= \frac{\Delta_{ij}}{\sum_{j \in b_i^t} \Delta_{ij} + s} \\ \gamma_j &= \frac{\frac{1}{d_{ij}}}{\sum_{j \in q_i^t} \frac{1}{d_{ij}}} \end{aligned} \quad (10)$$

s is a small additive term to prevent the case when the denominator is equal to 0. The weights α_j^t and β_j^t represent the intensity of passenger demand at time t and the weight γ_j corresponds to the distance of request from node i . These weights help our proposed model to prioritize the embeddings that are geographically or semantically closer to node v_i at time t .

Table 1 provides a comprehensive summary of the notations used throughout the study.

4.2. Temporal Attention Layer

After the data is filtered through the spatial attention layer, we get a low-level vector that carries information about all the neighborhood nodes and has an overview of the spatial dependencies of the graph. In order to capture the temporal dependencies among the learned representations, these node embeddings are exchanged with time-based neighbors using a temporal attention layer. The embeddings are exchanged

through the scaled dot attention mechanism which will be described in detail next. This layer has 4 channels: the first and second channels analyze the dependencies among requests that arrive in the preceding and consecutive hour of the previous 7 days, and the third channel finds out dependencies among requests from the same hour of the previous 7 days. These three channels capture the linear dependencies that arise due to the regular patterns in data like the morning and evening rush hours. However, there could be non-linear dependencies which show up due to the recent events that might have taken place at the preceding time intervals or that reveal the travelling patterns of people. These dependencies are monitored by taking the data from previous h hours, where the value of h is determined through experimental evaluations. Their value provides an indication of customer flow in the region around the time request arrives and thereby helps our proposed model to capture the patterns apart from the morning and evening hour data repetition trends that are found in the existing studies.

The temporal attention layer determines the dependencies between the embeddings of different time slots through the use of the scaled dot attention mechanism which has been found to capture the dependencies among graphs in a better manner than the self-attention mechanism Wang et al. (2021b). Figure 6 illustrates the mechanism followed by the scaled dot attention layer in determining the importance of embedding from a particular time slot. It gets as input the initial embeddings E^{t+1} of all the grid cells at the time slot $t + 1$ when prediction needs to be done, and the embeddings E^t of the previous time slot t whose weightage or importance needs to be determined. These embeddings are passed through the learnable weight matrices W^Q and W^K called the query and key matrices respectively. These learnable matrices act as a neural network and provide a better representation of the embeddings. The similarity between the embedding E^{t+1} and E^t is measured through the use of a dot product, which produces a similarity matrix S whose elements s_{ij} measure similarity between the i^{th} grid cell at time slot $t+1$ and j^{th} grid cell at time slot t . A high dot product value suggests dissimilarity between the embeddings, while a low value indicates similarity. However, the dot product can produce values across a wide range, potentially leading to some values that are excessively large, consequently causing vanishing gradient issue. To mitigate this, scaling is applied to reduce the magnitude of these weights. After scaling, the value of this weight comes out to be any number between $-\infty$ to ∞ whereas the weights in the attention mechanism are between 0 and 1. Therefore, these weights are normalized using the soft-max function, resulting in the values in the desired range of 0 to 1. These weights measure the affinity between the grid cells at time $t + 1$ with all the grid cells at time t . They are thereupon multiplied with the projected embeddings E^t passed through the learnable weight matrix W^V , called the value matrix. Through this approach, the proposed system obtains an updated representation for each time slot t by selectively focusing on grid cells that are similar to it. The above procedure calculated the importance of embeddings at a particular time slot. However, the temporal dependency arises due to the 3 linear layers and 1 non-linear layer, and there are multiple time slots in one layer. For instance, the non-linear layer contains the spatial embeddings of previous h hours, and the linear layers contain the spatial embeddings of previous 7 days. Thus for each layer, the proposed model sums the representations of all the time slots in order to obtain the temporal representation of the entire particular layer. Upon acquiring the embeddings for each layer, the proposed model consolidates this information into a unified spatio-temporal representation by incorporating another self-attention unit across all four layers.

After describing the procedure for determining the importance of temporal embeddings we describe the non-linear dependencies that arise due to the contextual data

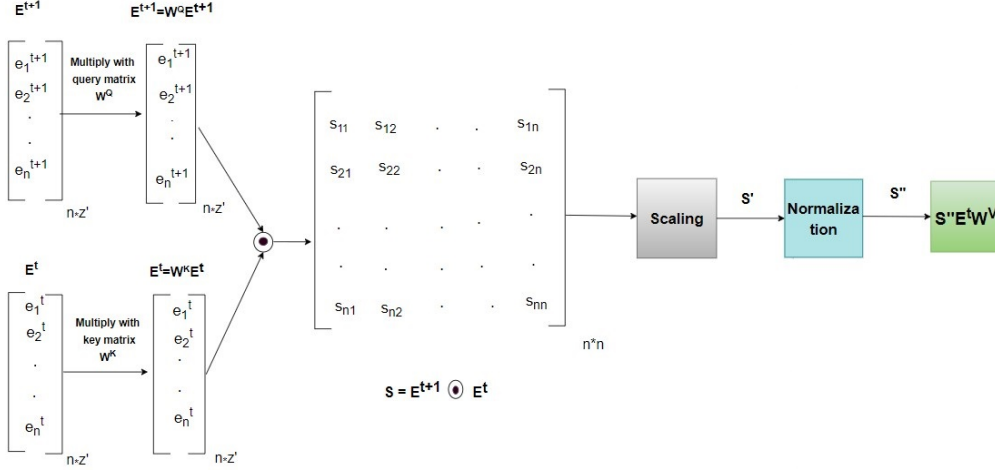


Figure 6.: Scaled dot attention for calculating affinity between temporal embeddings

and travelling patterns of people in detail next.

4.2.1. Context-aware data

Context-aware data refers to the data about the surrounding environment of a location and it provides an indication of the events that might have taken place around that location. This data is collected through various software and hardware tools and it has been used to modify the behavior of various systems. In the case of ride-hailing platforms, context-aware data can be used to direct the routes to users, considering the local events that might have taken place around that place. For instance, if the context-aware data displays that there is road construction in the area, then the vehicles are recommended to divert their route and travel through a different path in order to ensure the passengers reach their destination on time. Similarly, if the context-aware data displays that the area is free from traffic jams, then the vehicles are directed towards that route to provide the users with a hassle-free transportation service. Various works have been done that have used context-aware data to direct safe Galbrun, Pelechrinis, & Terzi (2016), pleasant de Souza, Pedrosa, Botega, & Villas (2018), or personalized routes Shan, Zhou, & Wang (2018) to the users. These works have used this data to modify the behavior of the system and direct users towards the routes that take into account the local condition of the place.

Our proposed model also uses context-aware data to capture the events that might have taken place around the location at a particular period of time. However, in our proposed model the data is not gathered from the software and hardware tools. Rather it is collected by the non-linear channel of the temporal attention layer. This layer captures all the customer requests that have arrived in that area for the preceding h hours and uses that to analyze the local environment of that place. The data from preceding h hours provides an indication of one of the following things: sparsity or density of requests in the area or the occurrence of an event at that place.

If the data for the past h hours shows that there are few requests in the area,

there may have been some impulsive event that reduced the flow of requests in and out of the area. This event could correspond to heavy rainfall, snowfall, or a security breach in that area. If there are no events scheduled at the place and the customer demand is still low then the area may have few requests, to begin with, meaning that people in that area do not use ride-hailing platforms for their daily commute. In both cases, there is a high probability that the area will have few requests in the next hour. This context-aware data thus helps our proposed model to anticipate future requests according to the local conditions of the place. Similarly, if the previous hours are abundant in requests, there might be an upcoming event in that area - a football game, festival sale, or any other event that influences passengers. However, if there are no events scheduled and the customer demand is high, it reveals that the area is dense in requests and there is always a higher flow of passengers in and out of that area. These patterns reveal important contextual information and can be used to monitor the flow of passengers in the region. They help our proposed model to capture local events that might have taken place around the location where the request needs to be predicted. These dependencies are captured by the non-linear channel of the temporal attention layer.

4.2.2. Travelling Behavior

Non-linear dependencies can also arise due to the travelling patterns of people. According to a behavioral study, people spend 5 to 6 hours outside of their homes during holidays Diffey (2011), which can include time spent in their garden, walking, or travelling in cars. Thus, after this time-period people tend to return to their original location by using any mode of transportation. This suggests that requests start to recur after this time and these patterns can be exploited to predict future requests. Further, during weekdays people go to their homes after their office hours are complete. As data from various countries reveals that people spend on average 2 – 6 hours in their workplace Ortiz-Ospina (2020) this pattern can be exploited to predict the travelling behavior of people during weekdays. Moreover, there are other recurring patterns such as shopping Ortiz-Ospina (2020), etc, which can be used to predict the future occurrence of requests. Thus, the data from previous hours provides an indication of travelling behavior of people and it reveals their office hours, recreation time, shopping hours, and other hobbies that can be used to predict future requests. This behavior is captured by the non-linear channel of the temporal attention layer and it provides insights into the recurring pattern of requests in ride-hailing platforms which can be used to predict the future occurrence of requests.

4.3. Transferring Attention Layer

After the data is modelled for spatial and temporal patterns, we pass it through the feed-forward neural network layer to get the number of requests at each node of a graph which represents the demand in the region. However, the proposed model fine-tunes the output like Shen et al. (2022) with the output of the historical average to obtain better results through the use of a weighted aggregator. The resultant demand is represented as a matrix $\hat{\delta} = \{\hat{\delta}_1, \hat{\delta}_2, \dots, \hat{\delta}_n\}$. In order to represent the origin and destination of requests, the transferring attention layer is used which models the transmission from one node to another based upon the transferring probability p_{ij} . p_{ij} represents the probability that requests are transferred from node i to node j and it is mathematically

represented as

$$p_{ij} = \frac{\exp(\text{AN}(e_i^T, e_j^T))}{\sum_{i=j}^n \exp(\text{AN}(e_i^T, e_j^T))} \quad (11)$$

OD pair ($\hat{\Delta}_{ij}$) is calculated from demand by using transferring probability p_{ij} as follows:

$$\hat{\Delta}_{ij} = \hat{\delta} \cdot p_{ij} \quad (12)$$

Like demand prediction, the output is fine-tuned with the weighted aggregator Shen et al. (2022) to obtain better prediction results.

5. Prototype Implementation

In this section, we evaluate our proposed model based on extensive simulations.

Datasets

Table 2.: Summary of Datasets used

Datasets	New York	Washington DC
Time Span	1 month	1 month
Grid cell size(default)	2.5 km	2.5 km
Number of grid cells	361	63
Time slot granularity	1 hour	1 hour

We conduct experiments to determine the parameter settings on the real-world taxi dataset generated from New York City. After that, we verify the parameter setting on the Washington DC dataset. Table 2 provides a summary of the datasets used for the experimental evaluation of our proposed model. The dataset is divided into grid cells of lengths 2.3, 2.4, 2.5, 2.6 and 2.7 km and the experiments are conducted on these sizes of grid cells. The default length of the grid cell is set as 2.5 km (it is discussed in detail in subsection 5.1). The datasets were collected for the months of February 2016 and 2017 respectively. Each dataset is divided into grid cells of 2.5 km with a time gap of 1 hour. The 1 hour time interval is chosen because it corresponds to the movement patterns of people Wang et al. (2021b). For instance, rush hours typically refer to specific peak traffic times during the day, which occurs within this hourly framework. Moreover, using a 1-hour time slot enables the prediction model to perform one cycle of gradient descent and facilitates the optimizer in efficiently assigning vehicle requests.

The rows of the dataset are of the form pick-up time, pick-up latitude and longitude, drop-off latitude and longitude, and passenger count. This data about passengers' origin and destination is fed as input to the GNN-based model and it predicts the number of requests that can arrive between any two locations within the next 1 hour.

Experimental Settings

In the experimental work, we used 75% of data for training purposes and kept the remaining 25% for testing purposes. In the training settings, 10% of data is used as a validation dataset and is used for hyperparameter testing. We implement our model with PyTorch 1.11.0 on Python 3.9. All the simulations were run on Windows i7 with 16 GB RAM for 200 epochs. The model was trained with a batch size of 1 and a

learning rate of 0.001. Based on these parameters, we evaluate the working of our proposed model.

Evaluation metrics and Loss function

We evaluate the prediction accuracy of our proposed model based upon the two widely applied metrics: Mean Absolute Percentage Error (MAPE) and Mean Absolute Error (MAE) which are defined as:

$$MAPE = \frac{1}{m} \sum_{i=1}^m \left| \frac{\hat{y}_i - y_i}{y_i + 1} \right| \quad (13)$$

$$MAE = \frac{1}{m} \sum_{i=1}^m |\hat{y}_i - y_i| \quad (14)$$

where m denotes the number of examples, \hat{y}_i denotes the predicted result and y_i represents the actual result. We estimate the performance of our proposed model on areas with varying levels of customer base and accordingly calculate MAPE-0, MAPE-3, and MAPE-5 where 0, 3, and 5 denote the minimum number of requests in different areas. We have used this threshold to see the patterns in different areas according to their customer base.

The loss function used by our proposed model is *SmoothL1Loss* Wang et al. (2021b), which is a variant of the mean-squared-error loss that employs a squared term when the absolute element-wise error falls below 1 and L1 loss otherwise. It provides a smooth transition in the loss computation and ensures a balanced impact on the model’s training. By adapting to the magnitude of the errors, the loss function effectively handles both small and large deviations, enhancing the model’s overall performance and accuracy. This allows for more stable and reliable convergence during the optimization process.

5.1. Grid cell length

The length of a grid cell is an important parameter that decides the complexity and accuracy of the proposed model. If the length is large, then the origin and destination of the majority of requests will be concentrated within a single grid cell and the OD prediction will reduce to demand prediction. If it is narrow, the time complexity of the model increases. Thus the length of a particular grid cell is an important parameter and needs to be determined.

Table 3 displays the performance of the proposed model based upon the parameters of MAPE and MAE, with the increase in length of a grid cell. There is a rapid decrease in the error of the model when the length increases from 2.3 km to 2.5 km. After that, the error becomes stagnant for the grid cells of length 2.5 km and 2.6 km. Thereafter, the error is found to increase again. The main perspective behind this behavior can be the change in data size and the number of neighbors on the varying lengths of grid cells. When the length of grid cell is small, there are multiple cells with no requests, and the spatial dependencies are not represented accurately by this size. Moreover, with small length time complexity of the model is high. However, when the length of grid cell increases, dataset size decreases, and the number of different neighbors changes which brings about an increase in error. Further, with an increase in grid cell

Table 3.: Simulation to check the length of a grid cell

Task	Grid cell length (km)	MAPE-0	MAPE-3	MAPE-5	MAE-0	MAE-3	MAE-5
OD	2.3	0.4191	0.4036	0.3838	5.8907	15.3091	19.3616
	2.4	0.3913	0.3646	0.3466	5.8756	15.3788	19.5304
	2.5	0.3866	0.3488	0.3269	5.4249	14.0479	17.7843
	2.6	0.3876	0.3513	0.3299	5.4508	14.1229	17.8809
	2.7	0.3985	0.3850	0.3715	6.4091	16.9501	21.5885
Demand	2.3	0.4350	0.3880	0.3671	53.7656	94.1438	106.8488
	2.4	0.4173	0.3688	0.3466	60.7930	106.6110	121.0631
	2.5	0.4222	0.3612	0.3354	46.7006	81.6304	92.5871
	2.6	0.4237	0.3627	0.3362	46.7409	81.6977	92.6591
	2.7	0.4405	0.3918	0.3717	60.4972	106.0421	120.4107

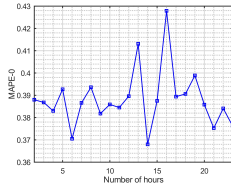
length, the OD task is found to converge to demand prediction. Thus the optimal value of the length of grid cells needs to be determined which reflects passenger mobility and performs effectively in a time-bound manner. Based on the experiments we have set the length of the grid cells as 2.5 km for our proposed model as it performs well under all the evaluation metrics.

In summary, the experimental evaluation determined the grid cell size based on the spatial dependencies among locations and it was found that the decrease in grid cell size does not always increase the prediction accuracy of the model which can be attributed to complex spatial dependencies among different locations. It’s worth noting that ride-hailing platforms define their grid cell size based on a range of performance optimization factors, tailoring it to specific applications. However, the value determined by our proposed model can be adopted by other models when accuracy in prediction is of paramount importance, even if it means removing some finer-grained road details in favor of overall performance enhancement.

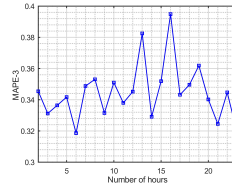
5.2. Non-linearities

The non-linearities in our proposed model are captured by the fourth channel of the temporal attention layer. This layer monitors the data from previous h hours and gives an indication of the events that might have taken place around the location during these hours. However, to properly monitor the events around that place, the value of h needs to be determined through simulations. Figures 7, 8, 9 and 10 show the MAPE and MAE of the proposed model for OD and demand prediction with varying time hours. As can be seen through these figures, when the data from the previous 3 – 6 hours is used, the model is found to perform well under all the evaluation metrics. Particularly, the data from the previous 6 hours is found to perform best under all conditions.

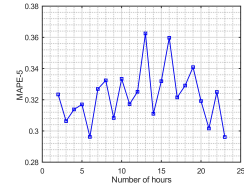
As already stated, the non-linear data provides context-aware information about the location and determines the average flow of requests in the area over a period of time. For instance, if the data from the previous 3 – 6 hours contains few requests



(a) MAPE-0 for OD prediction

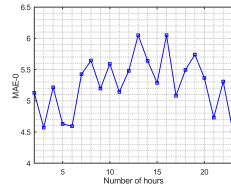


(b) MAPE-3 for OD prediction

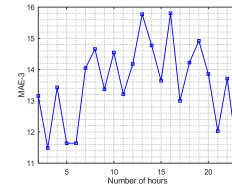


(c) MAPE-5 for OD prediction

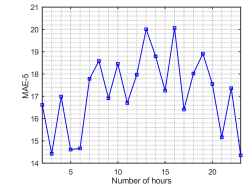
Figure 7.: MAPE for OD prediction



(a) MAE-0 for OD prediction

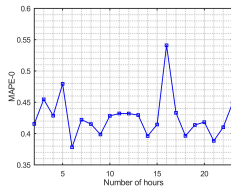


(b) MAE-3 for OD prediction

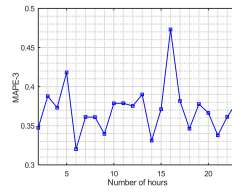


(c) MAE-5 for OD prediction

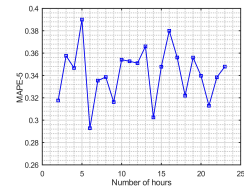
Figure 8.: MAE for OD prediction



(a) MAPE-0 for demand prediction



(b) MAPE-3 for demand prediction



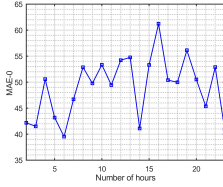
(c) MAPE-5 for demand prediction

Figure 9.: MAPE for demand prediction

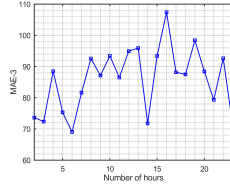
then that area may be sparse or some event may have occurred like rainfall, security breach, etc which reduced the flow of requests to that area. Similarly, if the previous hours have more requests then that area will either be high-demand area or some event might be scheduled at that place which has increased its demand.

However, among the past 3 – 6 hour data, the data from the previous 6 hours is found to perform best under all the evaluation metrics. The intuitive explanation might be that it reveals the travelling behavior of people and represents the average time spent outside by users.

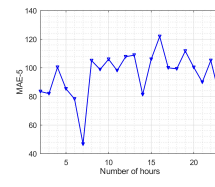
As the office timings in different countries vary from 2 – 6 hours Ortiz-Ospina (2020) and the demand re-arises after this time period, it provides one of the explanations for the data from the previous 6 hours to perform well. Moreover, a behavioral study



(a) MAE-0 for demand prediction



(b) MAE-3 for demand prediction



(c) MAE-5 for demand prediction

Figure 10.: MAE for demand prediction

Diffey (2011) has found that on average people spend 5 – 6 hours outside their homes during holidays (it can include time spent in their garden, time doing walk or travelling in cars). It provides further explanation for using previous 6 hour data to model non-linearity. Thus, from experimental studies and behavioral patterns of people, we conclude that data from previous 6 hours reflects passenger mobility well and gives an indication of customer re-appearance over different areas.

Data from previous 20 – 23 hours is also found to perform well, in particular for OD prediction tasks as can be seen through Table 4 and Figures 7 and 8. The main insight that we get from this pattern is the repeating sequence of requests the following day. As the 23 hour data captures the average flow of requests for a day and this pattern repeats the following day, the origin and destination of requests are predicted accurately.

Thus we conclude that data from previous 6 hours reflects the passenger travelling behavior and provides the contextual data of that place which can be used to analyze dependencies and predict the future demand and OD pair of requests in that area. Whereas the data from the previous 23 hours captures the repeating trend in requests and uses that to predict the future OD pair.

Table 4.: Repetition pattern of requests

Task	Ho- urs	MAPE- 0	MAPE- 3	MAPE- 5	MAE-0	MAE-3	MAE-5
OD	6	0.3705	0.3186	0.2962	4.5922	11.6408	14.6635
	23	0.3762	0.3200	0.2961	4.5285	11.4151	14.3549
Demand	6	0.3781	0.3201	0.2928	36.3080	61.8143	70.1092
	23	0.4493	0.3797	0.3479	40.9023	71.3015	80.7730

Importance of non-linear layer

We assess the significance of the non-linear layer and determine the impact of its inclusion on the performance of our proposed model. Table 5 shows the performance of the proposed model on different evaluation metrics based on the non-linear layer. The performance of the proposed system improves considerably with the inclusion of non-linear layer both in the OD and demand prediction tasks as can be seen through the evaluation metrics displayed in the table. This is because the non-linear layer captures the travelling behavior of people and provides contextual information of the place which indicates the request flow over preceding time frames. This information provides an indication of local commuter patterns in different areas which enhances

Table 5.: Significance of non-linear layer

Task	Non-linear layer	MAPE-0	MAPE-3	MAPE-5	MAE-0	MAE-3	MAE-5
OD	Yes	0.3705	0.3186	0.2962	4.5922	11.6258	14.6635
	No	0.4791	0.58655	0.59735	4.6253	11.6408	14.5918
Demand	Yes	0.3781	0.3201	0.2928	36.3080	61.8143	70.1092
	No	0.43515	0.4048	0.387	38.7564	67.5454	76.5284

the prediction accuracy of the proposed model.

5.3. Parameter setting verification with different models and data distributions

In this subsection, we determine the performance of the proposed model and compare it with the other models which have kept different parameters for the linear and non-linear layers. In order to check the parameter working, we have implemented these models with the GNN framework and set forth their parameters. Table 6 shows the performance of the proposed model (PM) and the baselines DL Ke et al. (2021) FL Hu et al. (2023) with different parameter settings. As can be seen through the table the proposed model surpasses the existing models in their performance. This is because of the use of linear and non-linear dependencies to capture the patterns among requests. The proposed model determines the linear dependencies by using the data from the previous, same, and next hours of the previous 7 days. Concurrently, non-linear dependencies are identified through data derived from the preceding 6 hours, which provides an accurate reflection of travel-related information while also offering insights into the contextual characteristics of the location. In contrast, previous models Hu et al. (2023); Ke et al. (2021), either solely relied on non-linear data Hu et al. (2023) or exclusively considered data from the same hour of the previous day and week Ke et al. (2021) to capture linear trends within the data. Additionally, they Ke et al. (2021) limited their analysis to data from the past 2 hours for understanding non-linear trends. These settings do not capture all the trends in underlying data, such as the travelling behavior of people or the contextual patterns of previous hours, and result in lower performance based on the evaluation metrics. The error rate is particularly high using FL Ke et al. (2021) since their model only utilizes the data from previous 11 hours to predict the future demand and does not capture the linear repeating trends in data.

In addition to verifying parameter settings using the New York dataset, we conducted a rigorous evaluation using the Washington DC dataset to assess the accuracy of non-linear dependencies through the data from the previous 6 hours. The findings, summarized in Table 7, showcase the performance of our proposed model in comparison to various baseline models on the Washington DC dataset. These results not only demonstrate the superiority of our proposed model but also underscore its ability to optimize parameter values for both linear and non-linear dependencies. Importantly, this evaluation underscores the adaptability of our model to different data distribution patterns, particularly evident in the context of Washington DC’s significantly lower

Table 6.: Parameter verification on New York dataset

Task	Method	MAPE-0	MAPE-3	MAPE-5	MAE-0	MAE-3	MAE-5
OD	DL	0.6829	0.9065	0.9362	21.9279	60.7931	78.5582
	FL	0.5417	0.4665	0.4517	54.9381	93.6856	106.3079
	PM	0.3705	0.3186	0.2962	4.5922	11.6408	14.6635
Demand	DL	0.6829	0.9065	0.9362	21.9279	60.7931	78.5582
	FL	0.4634	0.4472	0.4250	37.4200	65.0224	73.6000
	PM	0.3798	0.3372	0.3183	36.3080	61.8143	70.1092

Table 7.: Parameter verification on Washington DC dataset

Task	Method	MAPE-0	MAPE-3	MAPE-5	MAE-0	MAE-3	MAE-5
OD	DL	0.4771	0.5351	0.5483	3.2218	10.1279	13.6659
	FL	0.5685	0.5745	0.5581	12.0491	32.6828	42.0089
	PM	0.4107	0.4341	0.4551	2.4989	7.5256	10.1133
Demand	DL	0.5523	0.5713	0.5802	21.0160	37.9087	43.8728
	FL	0.5854	0.6181	0.6257	158.1532	272.0564	309.5320
	PM	0.3798	0.3681	0.3474	10.2358	18.0736	20.6880

request volume when contrasted with the New York dataset.

5.4. Prediction accuracy with different time slot granularities

The effectiveness of the proposed model depends upon the granularity of the time slots used for prediction. As depicted in Figure 11, the system’s performance exhibits variations across different time slot granularities. Notably, the performance of the proposed model displays improvement as the time slot granularity increases. This can be attributed to the higher data points within each time slot with the increase in time slot granularity which results in lower prediction error. Apart from this, the other reason for higher error rates in smaller time slots can be attributed to high sensitivity to short-term fluctuations and noise in the data which makes it challenging to make accurate predictions. With larger time slots this variability in data gets smoothed out, which makes it easier for the system to determine the underlying trends.

5.5. Visual comparison of predicted and actual values

Figure 12 provides a visual comparison of predicted and actual values of passenger requests. In this figure, x -axis represents the actual number of requests, y axis represents the predicted number of requests, and the plot shows the relation between the actual and predicted values. As can be seen through the figure, the values predicted by the proposed model are closely related to the actual values. This shows that though the error rate is high and is close to 40% the proposed model predicts the areas with

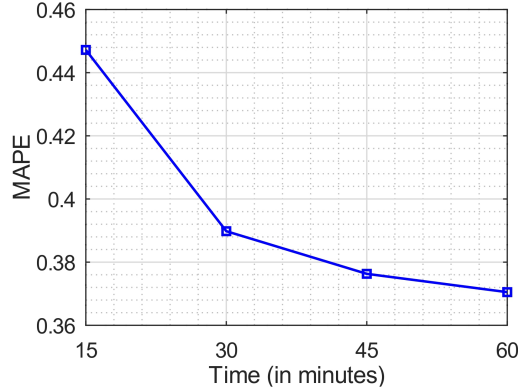


Figure 11.: MAPE with varying time slots

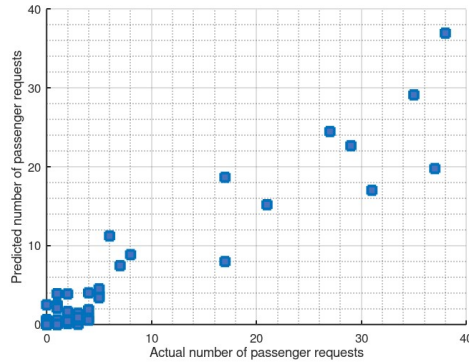


Figure 12.: Predicted and actual values of passenger requests

high and low requests very well which indicates the ride-hailing platforms about the request flow in different regions. These platforms can use this data to allocate vehicles to different areas according to the demand in that area.

5.6. Comparison with previous models

We evaluate the performance of our proposed model by comparing it with the following baselines:

GCRN Seo et al. (2018): It captures the spatial dependencies and dynamic patterns in ride-hailing requests through GCN and RNN.

GEML Wang et al. (2019): It captures the spatio-temporal dependencies in ride-hailing requests through GCN and LSTM.

Gallat Wang et al. (2021b): It predicts the origin and destination of requests through GNN.

BGARN Shen et al. (2022): It predicts the origin and destination of requests through GNN and RNN.

Table 8 displays the performance of GCRN, GEML, Gallat, BGARN, and our proposed model (PM) on all the evaluation parameters on the New York dataset. The table displays that the proposed model performs better under all the metrics. This is because we have used context-aware data and analyzed the travelling pattern of users and used that to predict the future occurrence of requests. These patterns reveal the reason behind the non-linear temporal dependencies that arise in data and when these

Table 8.: Comparison on OD and demand prediction for different methods on New York dataset

Task	Method	MAPE-0	MAPE-3	MAPE-5	MAE-0	MAE-3	MAE-5
OD	GCRN	0.5829	0.7853	0.8216	20.2301	57.3207	74.3299
	GEML	0.6732	0.8825	0.9066	19.6102	54.0873	69.7505
	Gallat	0.6654	0.8756	0.8996	19.2130	53.9155	69.6235
	BGARN	0.3866	0.3488	0.3269	5.4249	14.0479	17.7843
	PM	0.3705	0.3186	0.2962	4.5922	11.6408	14.6635
Demand	GCRN	0.7234	0.6216	0.5821	105.4090	184.7915	209.8527
	GEML	0.6214	0.6203	0.6277	161.2817	277.3443	315.5562
	Gallat	0.5872	0.5265	0.4943	69.3909	121.4460	137.7934
	BGARN	0.4222	0.3612	0.3354	46.7006	81.6304	92.5871
	PM	0.3798	0.3372	0.3183	36.3080	61.8143	70.1092

patterns are paired with the linear patterns like the morning and evening rush hours the model is found to capture different types of dependencies and thereby surpass the existing models in performance.

5.7. Navigating Errors: Unveiling Model Strengths Despite Challenges

In the realm of on-demand ride-hailing services, accurately predicting the number of passenger requests at a particular time and location is a notable challenge. This challenge stems primarily from the intricate and multifaceted nature of human behavior, which is influenced by various factors. These factors encompass users' willingness to travel, local weather conditions, and traffic congestion. While our model has successfully captured certain facets of human behavior, such as travel patterns, through its non-linear layer, there are several other behavioural patterns which are not been explored and affect the prediction accuracy of the proposed model. In this subsection, we will first analyze the distribution of errors and thereupon reveal the strengths of the proposed model.

The histogram presented in Figure 13 illustrates the relationship between the MAPE and the count of requests within specific grid cells. The x -axis of the plot denotes the request count on a grid cell, while the y -axis represents the corresponding MAPE. It can be seen through this figure that the error decreases with the increase in the number of requests that appear at a grid cell. When the number of requests is low for a specific grid cell, the difference between the predicted and actual values has a more pronounced impact on the calculated error rate. This is because the relative magnitude of errors is higher when the denominator (request count) is small. In contrast, as the request count increases, the impact of individual errors diminishes relative to the total number of requests. Consequently, the error rate tends to decrease with a higher request count. This pattern is consistent with statistical principles, where larger sample sizes generally lead to more stable and representative measurements. Therefore, the observed trend in the figure highlights the importance of considering request count in the interpretation of error rates, emphasizing that low request counts may result in disproportionately higher error rates, while larger request counts contribute to more reliable and representative error metrics.

However, it is essential to highlight that despite these inherent complexities, our

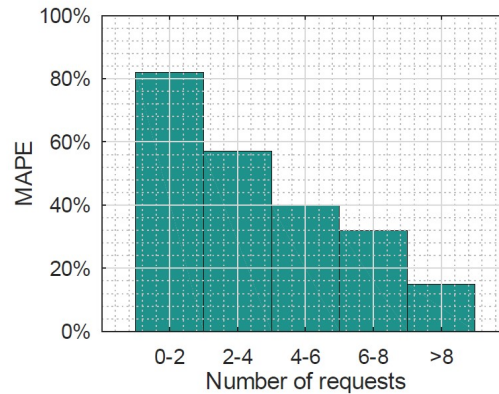


Figure 13.: Error distribution

proposed model has several significant strengths.

Identification of High-Demand Areas.

The proposed model's key strength lies in its ability to consistently identify areas with a surge in demand, even if the predicted passenger count may sometimes deviate from the actual count. This can be verified through Figure 12 which shows that even though the proposed model's values do not exactly match with those of actual values, it displays the demand patterns over different areas effectively. This capability allows the ride-hailing platforms to allocate drivers strategically to the high-demand areas, resulting in faster service, lower waiting times, and increased passenger satisfaction.

Mitigating surge pricing.

Surge pricing emerges when demand outstrips supply. The proposed model reduces it by providing insights into areas that are likely to experience high demand. This strategic approach encourages drivers to converge around these high-demand areas, ensuring a more precise equilibrium between passenger needs and driver availability.

Real-Time Adaptation.

The model's flexibility in utilizing previous hour data for real-time adjustments ensures that they can respond promptly to sudden spikes in demand, even when they deviate from initial predictions. This real-time adaptability maintains service responsiveness.

Data-Driven Decision Support.

Beyond prediction, the proposed model serves as a valuable tool for data-driven decision-making. It offers insights into historical demand patterns, aiding in driver-passenger matching and route optimization.

In conclusion, while predicting passenger numbers in the on-demand ride-hailing industry remains a challenge, our proposed model's strengths in identifying high-demand areas, reducing surge pricing, adapting in real-time, and facilitating data-driven decisions significantly enhance the efficiency and responsiveness of the service, resulting in an improved experience for both drivers and passengers. Although the model may occasionally predict a higher or lower demand than the actual number of passengers arriving, it has considerable strengths in determining the areas with high demand which can facilitate in smooth allocation of resources.

6. Applications

Ride-hailing services generate an enormous volume of passenger data every day. This data can be used effectively for predicting the future occurrences of passenger requests. This paper focuses on harnessing the power of GNN to make predictions regarding future origin and destinations of requests. The applications of such predictions are diverse and impactful. Some of them include:

Revenue optimization and passenger satisfaction: When the ride-hailing platforms are provided with data about the passenger’s origin and destination in advance, they can use this data to strategically dispatch drivers to the areas that will have high demand which results in efficient coverage of passenger requests. This approach leads to an increase in revenue of the platform as they are able to accommodate a larger number of passenger orders due to the presence of drivers in passenger-centric areas.

This data-driven approach also has a significant impact on passenger satisfaction. By dispatching drivers to areas with high demand, waiting times for passengers are reduced. As a result, passengers experience shorter wait times and are able to secure rides promptly, benefiting from the higher supply of drivers in high-demand regions.

Fleet Management: Fleet size refers to the number of vehicles required to service passenger requests that can arrive in a given area. By predicting the future origins and destinations of requests, ride-hailing companies get an advanced estimate of the vehicles required to cover the requests that arrive over different frames of the day. This will result in efficient resource utilization as the companies will use the higher resources when the demand is expected to be high and will constrain the resources over the time periods when the demand is expected to be low.

Eco-friendly rides: Ridesharing services result in eco-friendly rides as they pair multiple passengers with similar routes in a single vehicle. This results in efficient utilization of vehicles and decreases the count of vehicles on the road. However, the current statistics display that only 15% of rides are shared Petit (2020), whereas 73% of rides can be shared with a slight increase in the waiting time of passengers Cai, Wang, Adriaens, & Xu (2019). This highlights the substantial scope for improving ridesharing rates if accurate predictions of passenger origins and destinations are made in advance. By accurately forecasting the pickup and drop-off points of passenger requests, ridesharing platforms can proactively match passengers with similar routes, thereby increasing the likelihood of shared rides.

Traffic Planning: The predicted future demand and ride origins/destinations can contribute to traffic planning efforts. By analyzing these patterns, transportation authorities can gain insights into congestion-prone areas and make informed decisions regarding infrastructure improvements, traffic flow management, and public transportation planning.

Overall, the application of GNN-based models for predicting future demand, origins, and destinations offers numerous opportunities for improving operational efficiency, enhancing customer experience, and optimizing resource allocation in the dynamic landscape of ride-hailing services.

7. Conclusion

In this paper, we define passenger mobility through origin-destination prediction which is helpful in directing optimal routes to drivers and providing matching algorithms for drivers and passengers. OD prediction is complex in comparison to demand prediction

as it predicts the demand in a certain region and the destination of these demands. We have used GNN to capture the spatio-temporal dependencies among requests and predicted the OD pair of requests. We have particularly focused on temporal nonlinearities that arise due to contextual events or the travelling patterns of people. While modelling these dependencies, the length of the grid cell is an important parameter and it can regulate the neighborhood count. We have determined its value through extensive simulations. The parameters that decide the grid cell length and the nonlinearities are estimated for demand prediction models also. Extensive simulations determine superior performance by our proposed model as compared to the existing baselines.

References

- Cai, H., Wang, X., Adriaens, P., & Xu, M. (2019). Environmental benefits of taxi ride sharing in beijing. *Energy*, *174*, 503-508.
- Cho, E., Myers, S. A., & Leskovec, J. (2011). Friendship and mobility: user movement in location-based social networks. In *Proceedings of the 17th acm sigkdd international conference on knowledge discovery and data mining* (pp. 1082–1090).
- de Souza, A. M., Pedrosa, L. L. C., Botega, L. C., & Villas, L. (2018, June). Itssafe: An intelligent transportation system for improving safety and traffic efficiency. In *2018 IEEE 87th vehicular technology conference (vtc spring)* (p. 1-7).
- Diffey, B. L. (2011). An overview analysis of the time people spend outdoors. *British Journal of Dermatology*, *164*(4), 848–854.
- Galbrun, E., Pelechris, K., & Terzi, E. (2016). Urban navigation beyond shortest route: The case of safe paths. *Information Systems*, *57*, 160-171.
- Gao, J., Li, X., Wang, C., & Huang, X. (2022, Aug). Bm-ddpg: An integrated dispatching framework for ride-hailing systems. *IEEE Transactions on Intelligent Transportation Systems*, *23*(8), 11666-11676.
- Garg, N., & Ranu, S. (2018). Route recommendations for idle taxi drivers: Find me the shortest route to a customer! In *Proceedings of the 24th acm sigkdd international conference on knowledge discovery & data mining* (p. 1425–1434). New York, NY, USA: Association for Computing Machinery.
- Hamilton, W., Ying, Z., & Leskovec, J. (2017). Inductive representation learning on large graphs. *Advances in neural information processing systems*, *30*.
- Han, C., Song, S., Wang, C., et al. (2004). A real-time short-term traffic flow adaptive forecasting method based on arima model. *Journal of system simulation*, *16*(7), 1530–1535.
- Hu, S., Ye, Y., Hu, Q., Liu, X., Cao, S., Yang, H. H., ... Wu, C. (2023). A federated learning-based framework for ride-sourcing traffic demand prediction. *IEEE Transactions on Vehicular Technology*, 1-15. doi:
- Jin, G., Cui, Y., Zeng, L., Tang, H., Feng, Y., & Huang, J. (2020). Urban ride-hailing demand prediction with multiple spatio-temporal information fusion network. *Transportation Research Part C: Emerging Technologies*, *117*, 102665.
- Ke, J., Qin, X., Yang, H., Zheng, Z., Zhu, Z., & Ye, J. (2021). Predicting origin-destination ride-sourcing demand with a spatio-temporal encoder-decoder residual multi-graph convolutional network. *Transportation Research Part C: Emerging Technologies*, *122*, 102858.
- Lippi, M., Bertini, M., & Frasconi, P. (2013, June). Short-term traffic flow forecasting: An experimental comparison of time-series analysis and supervised learning. *IEEE Transactions on Intelligent Transportation Systems*, *14*(2), 871-882.
- Ortiz-Ospina, E. (2020). *How do people across the world spend their time and what does this tell us about living conditions?* <https://ourworldindata.org/time-use-living-conditions>. (Accessed: 2022-10-13)
- Petit, Y. L. (2020). *Uber pollutes more than the cars it replaces—us scientists.* <https://>

- www.transportenvironment.org/discover/uber-pollutes-more-cars-it-replaces-us-scientists/. (Accessed: 2022-02-28)
- Schaller, B. (2021). Can sharing a ride make for less traffic? evidence from uber and lyft and implications for cities. *Transport Policy*, 102, 1-10.
- Seo, Y., Defferrard, M., Vandergheynst, P., & Bresson, X. (2018). Structured sequence modeling with graph convolutional recurrent networks. In *Neural information processing: 25th international conference, iconip 2018, siem reap, cambodia, december 13-16, 2018, proceedings, part i 25* (pp. 362–373).
- Shan, D., Zhou, W., & Wang, J. (2018, July). A novel personalized dynamic route recommendation approach based on pearson similarity coefficient in cooperative vehicle-infrastructure systems. In *2018 ieee 8th annual international conference on cyber technology in automation, control, and intelligent systems (cyber)* (p. 1270-1275).
- Shen, J., Tziritas, N., & Theodoropoulos, G. (2022). A baselined gated attention recurrent network for request prediction in ridesharing. *IEEE Access*, 10, 86423–86434.
- Wang, Y., Yin, H., Chen, H., Wo, T., Xu, J., & Zheng, K. (2019). Origin-destination matrix prediction via graph convolution: A new perspective of passenger demand modeling. In *Proceedings of the 25th acm sigkdd international conference on knowledge discovery & data mining* (p. 1227–1235). New York, NY, USA: Association for Computing Machinery.
- Wang, Y., Yin, H., Chen, T., Liu, C., Wang, B., Wo, T., & Xu, J. (2021a). Gallat: A spatiotemporal graph attention network for passenger demand prediction. In *2021 ieee 37th international conference on data engineering (icde)* (p. 2129-2134).
- Wang, Y., Yin, H., Chen, T., Liu, C., Wang, B., Wo, T., & Xu, J. (2021b, nov). Passenger mobility prediction via representation learning for dynamic directed and weighted graphs. *ACM Trans. Intell. Syst. Technol.*, 13(1).